Electron transport properties and collision cross sections in C_2F_4

K. Yoshida[a] and S. Goto
Kitami Institute of Technology, 165 Koen-cho, Kitami 090-8507, Japan

H. Tagashira
Muroran Institute of Technology, 27-1 Mizumoto-cho, Muroran 050-8585, Japan

C. Winstead[b] and B. V. McKoy[c]
A. A. Noyes Laboratory of Chemical Physics, California Institute of Technology, Pasadena, California 91125

W. L. Morgan[d]
Kinema Research and Software, P.O. Box 1147, Monument, Colorado 80132

(Received 20 August 2001; accepted for publication 13 November 2001)

We have measured the electron drift velocity, longitudinal diffusion coefficient, and ionization coefficient in tetrafluoroethene (C_2F_4). Using these data and the results of *ab initio* calculations of the elastic, momentum-transfer, and neutral-excitation cross sections, along with measurements of the partial ionization cross sections, we have performed a swarm analysis in order to construct a self-consistent set of electron impact cross sections for C_2F_4. The swarm analysis consists of solutions to Boltzmann's equation for electrons in C_2F_4 for values of $E/N \leqslant 500$ Td and direct Monte Carlo simulation of electron transport in C_2F_4 for $500\ \text{Td} \leqslant E/N \leqslant 2000$ Td. We present an analysis and discussion of the sensitivity of cross sections derived from swarm data to uncertainties in the electron transport measurements. We also discuss the failure of the two-term spherical harmonic solution to Boltzmann's equation for $E/N > 500$ Td, which necessitated the use of Monte Carlo simulations for high values of E/N. © *2002 American Institute of Physics.*
[DOI: 10.1063/1.1433189]

I. INTRODUCTION

Modeling and simulation of plasma chemistries are important components of reactor and process design. Whether employing fluid models or particle-in-a-cell or Monte Carlo methods, modeling of these plasma chemistries relies on a knowledge of the relevant electron collision cross sections. Elastic or momentum transfer cross sections are needed for the plasma electrical conductivity, ionization, and attachment cross sections for the electron and ion densities, and dissociation cross sections for fragmentation and subsequent radical production from the parent feed gas. For most gases of interest, a scarcity of low-energy electron collision data compels modelers to rely on mutually inconsistent results drawn from disparate sources and even, employing intuition and analogy, to guess at cross section values. The resulting cross section sets are, apart from any other weaknesses, frequently inconsistent with electron swarm measurements. On the other hand, cross section sets developed from swarm data alone suffer from nonuniqueness that renders the individual cross sections so obtained suspect.

A clearly preferable alternative is to obtain data of high quality for the most important collision processes and then to produce, via a suitable process of adjustment, a cross section set that is consistent with electron swarm measurements. Here we present the results of a coherent and focused effort to generate a validated and self-consistent cross section set for modeling C_2F_4 plasmas. Making use of electron swarm measurements, of measured electron-impact ionization cross sections, and of electron collision cross sections calculated from first principles, we have constructed the desired set of cross sections for electron impact on C_2F_4. The electron swarm parameters we have obtained compare well with the very recent measurements of Goyette *et al.*[1]

The low carbon–carbon bond strength of C_2F_4 is attracting interest in its use as a feed gas for oxide etching.[2] C_2F_4 is also produced by electron impact fragmentation of c-C_4F_8, a widely used plasma-processing gas. A consistent cross section set may therefore prove useful in modeling various plasma processes.

In Sec. II we describe and present results from the electron swarm measurements. Section III describes the first-principles calculations of elastic, momentum transfer, and excitation/dissociation cross sections for electron impact on C_2F_4. Finally, in Sec. IV, we describe and present results from our swarm analyses, which yield the validated and self-consistent cross section set that we seek.

II. MEASUREMENT OF ELECTRON SWARM PARAMETERS IN C_2F_4

Two types of experiments, namely the steady-state Townsend (SST) experiment and a drift-tube experiment, have been conducted to obtain the ionization coefficient α/N, the electron mean-arrival-time drift velocity W_m, and the product of the electron longitudinal diffusion coefficient

[a]Electronic mail: yoshida@elec.kitami-it.ac.jp
[b]Author to whom correspondence should be addressed; electronic mail: carl@schwinger.caltech.edu
[c]Electronic mail: mckoy@its.caltech.edu
[d]Electronic mail: morgan@kinema.com

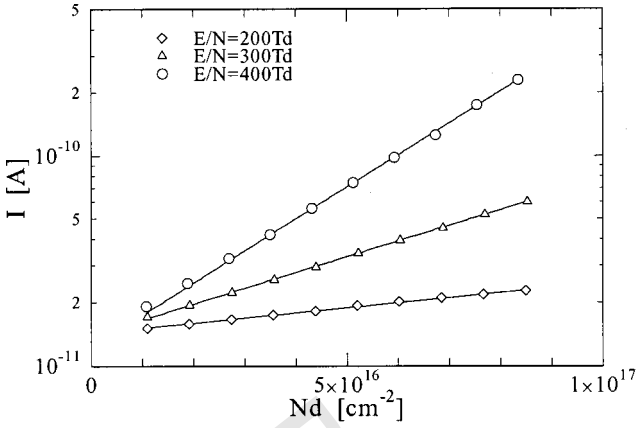

FIG. 1. Ionization current growth curve measured in C_2F_4.

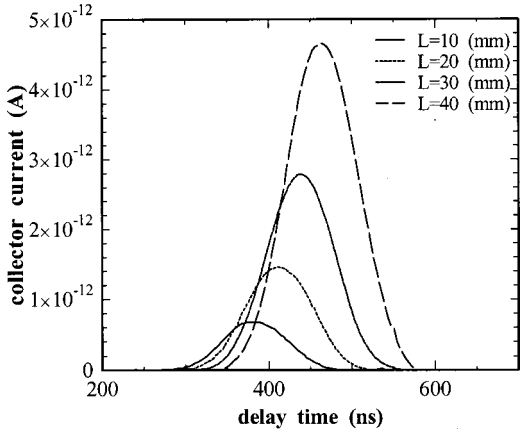

FIG. 2. Arrival-time spectra measured in C_2F_4 at $E/N=500$ Td.

and gas density ND_L in C_2F_4. The only other C_2F_4 swarm measurements available are the very recent measurements of Goyette *et al.*[1] They employed a pulsed Townsend experimental technique to measure electron drift velocities, ionization coefficients, and attachment coefficients at much lower values of E/N (electric field strength divided by gas number density) than those measurements presented here.

A. The experimental apparatus and analytical method

The experimental apparatus and analytical method used are the same as in the previous work.[3] The purity of C_2F_4 employed is more than 98%, according to the manufacturer (ABCR GmbH & Co. KG).

1. The SST experiment

The apparatus for the SST experiment is a conventional one, where two parallel plate electrodes, 150 mm in diameter and machined to the Harrison profile, are set in a stainless steel chamber. In the middle of the cathode, a quartz plate 20 mm in diameter and coated with a gold thin film is embedded to release initial electrons by the photoelectric effect. An electrometer is connected to the anode to measure the ionization current. The electrode separation and the pressure adopted in the present work range from 4 to 31 mm and 0.1 to 1.2 Torr, respectively.

Figure 1 shows examples of growth curves of the ionization current measured at relatively low E/N values as a function of the product Nd, where N is the gas density and d the electrode separation. The growth curves seem to be linear on a semilog plot. This fact may suggest that electron attachment is negligibly small in the E/N range of the present measurement.

Because the present SST experiment aimed to obtain the ionization coefficient α, the ionization current was measured only in the range of relatively small electrode separation where the effect of secondary electrons from the cathode did not strongly influence the current growth curve. In this case, the Townsend equation for the current growth curve reduces to $I=I_0e^{\alpha d}$, I_0 being the initial current. An analysis was performed to determine the coefficient α by applying a curve-fitting technique based on a least-square method.

2. The double-shutter drift tube experiment (the arrival-time spectra experiment)

A double-shutter drift tube was used to measure arrival-time spectra (ATS) of an isolated electron swarm at various positions in the drift space. The drift tube consists of a photocathode, a collector, two electrical shutters, and a guard electrode. The photocathode is the same as in the SST experiment except for size of the quartz plate (30 mm in diameter). The shutter consists of a pair of stainless steel grids with spacing of 1 mm. The grid has a large number of holes, each having an area of 0.64 mm^2, photoetched in a lattice pattern, whose optical transmissivity is about 80%. The guard electrode consists of 80 pairs of stainless steel rings and polytetrafluorethylene ring spacers, the thickness of which is 0.5 mm each. The inner diameter of the guard electrode is 100 mm. The collector was made of stainless steel plate 70 mm in diameter. The distance between the shutters is variable. The distance and the pressure adopted in the present work range from 5 to 50 mm and 0.1 to 0.6 Torr, respectively.

Figure 2 shows a typical example of the measured ATS of electrons. The spectra become intense and broad with drift distance due to ionization and longitudinal diffusion of electrons. Fluctuations in the spectrum profile are mainly due to perturbation of the measured current.

In the ATS theory, the electron transport equation in real space is expressed as follows:[4,5]

$$\frac{\partial n(z,t)}{\partial z}=\alpha^{(0)}n(z,t)-\alpha^{(1)}\frac{\partial n(z,t)}{\partial t}+\alpha^{(2)}\frac{\partial^2 n(z,t)}{\partial t^2}-\cdots, \tag{1}$$

where n is the electron density at position z and time t, and $\alpha^{(i)}$ $(i=0,1,2...)$ are the ATS coefficients defined as

$$\alpha^{(0)}=\frac{d(\ln N_z)}{dz}, \tag{2a}$$

$$\alpha^{(1)}=\frac{d\langle t\rangle}{dz}, \tag{2b}$$

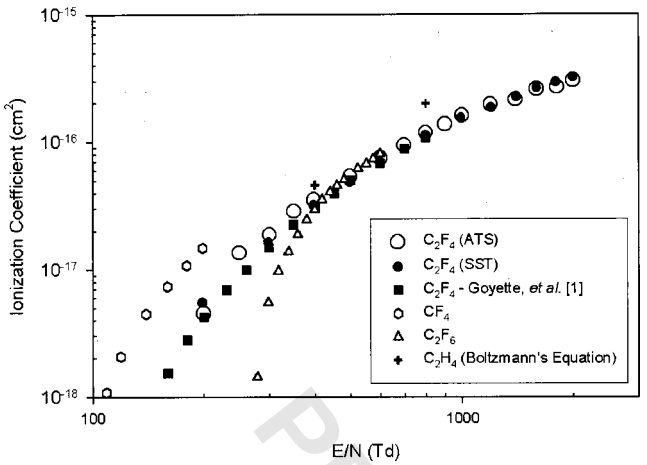

FIG. 3. The ionization coefficient.

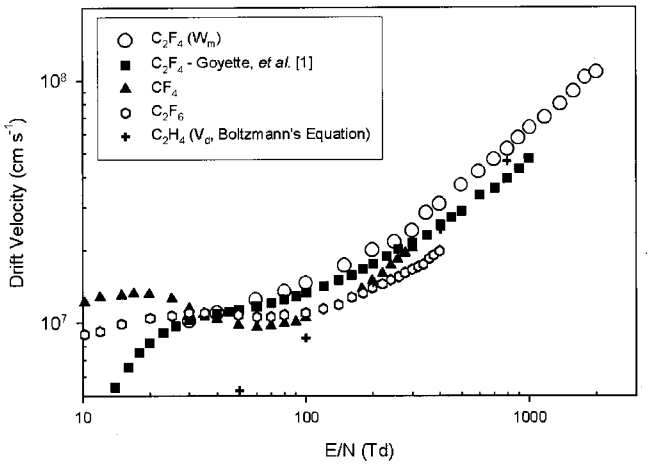

FIG. 4. The mean-arrival-time drift velocity W_m.

$$\alpha^{(2)}=\frac{1}{2!}\frac{d\langle T^2\rangle}{dz},\cdots \tag{2c}$$

where

$$N_z=\int_0^\infty n(z,t)dt,$$

$$\langle t\rangle=N_z^{-1}\int_0^\infty tn(z,t)dt,$$

$$\langle T^2\rangle=N_z^{-1}\int_0^\infty (t-\langle t\rangle)^2 n(z,t)dt.$$

Here N_z is the total number of electrons arriving at position z, and $\langle t\rangle$ is the first-order time moment of the ATS. The coefficients $\alpha^{(0)}$ and $\alpha^{(1)}$ correspond to the ionization coefficient and the inverse of the mean-arrival-time drift velocity W_m, respectively.[5] The relationship between $\alpha^{(2)}$ and the longitudinal diffusion coefficient D_L is given by[5]

$$\alpha^{(2)}W_m^3=D_L-3\alpha_T D_3+6\alpha_T^2 D_4-, \tag{3}$$

where D_3 and D_4 are higher-order coefficients than the longitudinal diffusion coefficient D_L in the conventional analysis of the electron transport equation.[6] In the present work, the longitudinal diffusion coefficient D_L was determined by neglecting the second- and higher-order terms in the above relation, as in previous work.[7] The ratio of the longitudinal diffusion coefficient to the electron mobility D_L/μ was calculated using the relationship $\mu=W_m/E$.

B. Results

Several measurements at each value of E/N were carried out under different conditions at room temperature.

1. The ionization coefficient

Figure 3 shows the ionization coefficient α/N obtained from the drift tube experiment combined with the ATS analysis (hereafter referred to as the ATS experiment) as open circles. The scatter of the measured data around the average value is less than about 4% except in a low E/N range. In Fig. 3, the α/N values obtained in the SST experiments are also shown along with the measurements of Goyette *et al.*[1] The two sets of measurements are nearly indistinguishable. The results of the ATS and SST experiments are seen to be in excellent agreement over an E/N range of 200–2000 Td, suggesting that the present measurements are correct. The coefficient α/N in C_2F_4 increases rapidly at an E/N of about 200 Td, then reaches a value of 3.1×10^{-16} cm^2 at E/N of 2000 Td. The E/N value at which the rapid increase of the coefficient α/N occurs is lower than that in C_2F_6 (Ref. 8) but higher than that in CF_4,[8] as seen in Fig. 3.

2. The mean-arrival-time drift velocity W_m

Several electron drift velocities have been theoretically defined depending on the principle of observation of an electron swarm. It has been noted, however, that these velocities, in principle, assume different values when the number of electrons in an isolated swarm is not conserved.[6] The mean-arrival-time drift velocity W_m was introduced as appropriate for the drift velocity observed in a drift tube experiment.[4,5]

Figure 4 shows the drift velocity W_m determined in the present work as well as the measurements of the drift velocity as defined by Goyette *et al.*[1] The latter lie somewhat below our mean arrival time measurements at higher values of E/N. For comparison, drift velocities in other gases are also plotted, although the definition of those velocities differs from that of the mean-arrival-time drift velocity. The drift velocity W_m in C_2F_4 monotonically increases with increasing E/N in the range of the present measurements, and its values are slightly greater than those of the drift velocities in CF_4, C_2F_6,[8] and C_2H_4,[9] in an E/N range of 50–2000 Td. The scatter of the measured values lies within about 4% of the average value except in a few cases.

3. The electron longitudinal diffusion coefficient ND_L

Figure 5 shows the electron longitudinal diffusion coefficient multiplied by the gas density ND_L. The coefficient increases with increasing E/N in the present measurements, although a relatively large fluctuation is seen. Scatter of the measured data around the average value reaches 40% at most. This is due to mainly fluctuations of the collector cur-

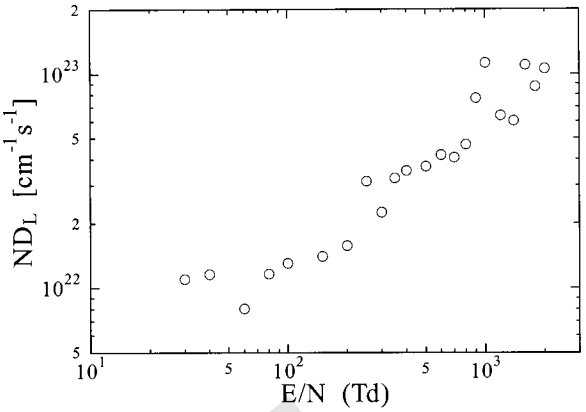

FIG. 5. The electron longitudinal diffusion coefficient.

rent, especially in the trailing edge of the ATS, since the trailing edge has a large weight in calculation of $\alpha^{(2)}$.

4. The ratio of longitudinal diffusion coefficient to electron mobility D_L/μ

The ratio of the electron longitudinal diffusion coefficient to the electron mobility D_L/μ is an important parameter often called the characteristic energy which, roughly speaking, is a measure of electron mean energy. Figure 6 shows the ratio D_L/μ deduced in the present work. The ratio D_L/μ is seen to increase monotonically from about 300 meV to 20 eV with increasing E/N in the present measurements. Roughly speaking, the scatter of all data around the average value in the drift tube experiment is limited to 4% for the ionization coefficient, 4% for the mean-arrival-time drift velocity, and 40% for the longitudinal diffusion coefficient. The ionization coefficient obtained in the ATS experiment is in good agreement with that obtained in the SST experiment. Electron attachment in C_2F_4 is not observed in the present work.

III. *AB INITIO* CALCULATIONS

Cross sections for elastic and electronically inelastic collisions between low-energy electrons and C_2F_4 were computed from first principles using the Schwinger multichannel

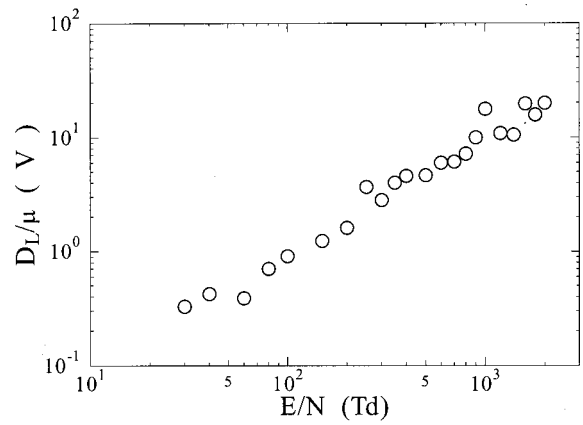

FIG. 6. The ratio of the longitudinal diffusion coefficient to the electron mobility.

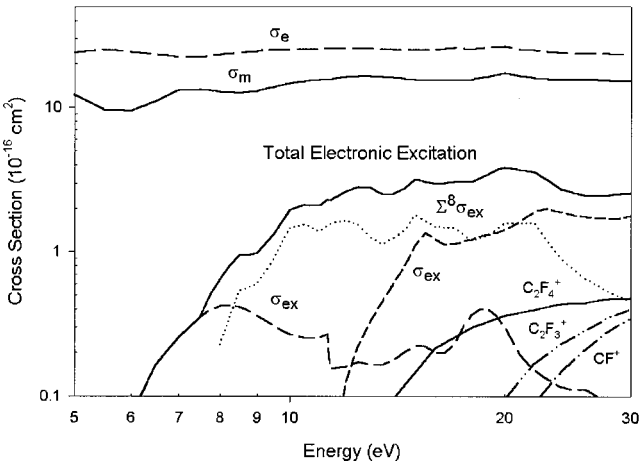

FIG. 7. Elastic, momentum transfer, excitation, and ionization cross sections for C_2F_4 for collision energies between 5 and 30 eV.

method[10,11] as implemented for parallel computers.[12,13] Details of the calculations and a more extensive discussion of the cross sections will be published separately.[14] Here we mention briefly some important features.

In carrying out the elastic calculations, we employed the so-called ''static-exchange'' approximation and, where resonances were involved, the ''static-exchange plus polarization'' approximation, both within the fixed-nuclei approximation. Additionally, at the lowest energies, an *ad hoc* correction was applied to remove an artifactual enhancement of the cross section typical of the static-exchange approximation. Generally speaking, this level of calculation is expected to do quite well for low-energy electron collisions. However, one consequence of the fixed-nuclei approximation is that vibrationally elastic and vibrationally inelastic scattering are not distinguished; moreover, any resonances in the fixed-nuclei elastic cross section tend to be sharper (narrower, and with a higher peak value) than in the experiment.

From elementary chemical considerations and from the strong analogy between C_2F_4 and the better-studied C_2H_4 molecule, it was possible to identify two electronic-excitation channels as particularly important. In both C_2F_4 and C_2H_4, the highest occupied molecular orbital (HOMO) is a π-type orbital that forms part of the carbon–carbon double bond, while the lowest unoccupied molecular orbital (LUMO) is the conjugate antibonding (π^*) orbital. The HOMO→LUMO excitation gives rise to a triplet state (often called the *T* state) and a singlet state (the *V* state). Excitation of the *T* state is important because of its very low threshold, 4.68 eV.[15] The *V* state has a considerably higher threshold, measured values being 8.84 eV Ref. 15 and 8.88 eV,[16] but it has a large oscillator strength (photoexcitation cross section), which typically implies that the electron cross section is also large.

Although the *T* and *V* excitations were expected (and turned out) to be most important individual processes, there exist other low-lying excited states of C_2F_4;[15] some of these even lie below the *V* state. Because these states, taken together, might contribute significantly to electron-impact excitation of C_2F_4, we computed cross sections for eight states

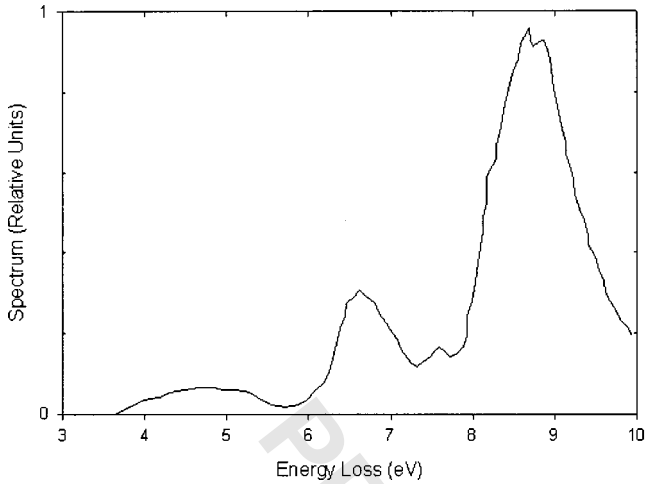

FIG. 8. Measured electron energy loss spectrum for 40 eV electrons in C_2F_4, from Ref. 15.

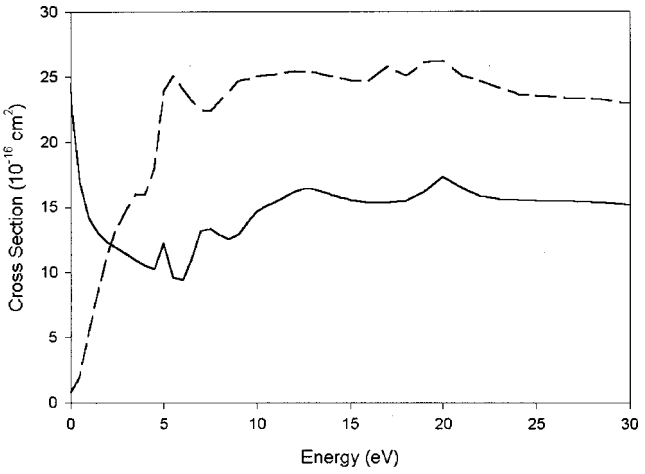

FIG. 9. Computed C_2F_4 elastic (dashed line) and momentum transfer (solid line) cross sections.

whose calculated thresholds lie below 10 eV. While the *T* state remained dominant in the summed cross section at the lowest energies, and the *V* state (because of its large transition dipole) remained dominant at the highest energies, we indeed found that, at intermediate energies, the eight other states make up a significant fraction of the summed excitation cross section.

IV. SWARM ANALYSIS AND RECOMMENDED CROSS SECTION SET

Figure 7 shows a summary of our calculated elastic and inelastic (excitation and dissociation) cross sections along with the ionization cross sections that have been measured by Haaland and Jiao.[17] Comparing this figure with the electron energy loss spectrum shown in Fig. 8,[15] the major energy loss features in the spectrum are seen to correspond to the cross sections shown in Fig. 7.

The cross section labeled ${}^8\sigma_{\mathrm{ex}}$ is the sum of eight excitation cross sections having energy losses of 8–10 eV. The calculated C_2F_4 dissociation energetics are shown in Table I.

The ionization cross sections shown for the $C_2F_4^+$, $C_2F_3^+$, and CF^+ products, which are the three largest, have been measured by Haaland and Jiao.[17] Their thresholds are 10.10, 15.85, and 13.86 eV, respectively. These excitation and ionization cross sections were the starting point for our swarm analysis.

TABLE I. C_2F_4 dissociation channels and energetics.

Dissociation products	Energy (eV)
CF_2+CF_2	3.06
CF_3+CF	4.52
C_2F_3+F	5.19
$C_2F_2+F_2$	7.09
C_2F_2+F+F	8.13
CF_2+CF+F	8.13
CF_3+C+F	9.79

A. Swarm analysis

The electron drift velocity calculated from the solution $f_0(\varepsilon)$ of Boltzmann's equation is defined as

$$V_d=\langle v_z\rangle=-1/3(2e/m)^{1/2}(E/N)\times\int[df_0(\varepsilon,E/N)/d\varepsilon]\varepsilon\,d\varepsilon/\sigma_m, \tag{4}$$

where ε is the electron energy, m is the electron mass, E/N is the electric field divided by gas number density ($\mathbf{E}=E\mathbf{z}$), f_0 is the electron energy distribution function, and σ_m is the momentum transfer cross section.

The *momentum transfer cross section* $\sigma_m(\varepsilon)$ is defined by

$$\sigma_m(\varepsilon)=2\pi\int\sigma_e(\varepsilon,\theta)(1-\cos\theta)\sin\theta\,d\theta, \tag{5}$$

where $\sigma_e(\varepsilon,\theta)$ is the differential cross section for elastic scattering. The momentum transfer cross section is also known in transport theory as the diffusion cross section. For a uniform differential cross section, i.e., $\sigma_e(\varepsilon,\theta)$ = constant, the elastic and momentum transfer cross sections are equal, i.e., $\sigma_m(\varepsilon)=\sigma_e(\varepsilon)$. When $\sigma_e(\varepsilon,\theta)$ is strongly peaked in the forward direction, $\sigma_m(\varepsilon)<\sigma_e(\varepsilon)$, and when it is peaked in the backward direction $\sigma_m(\varepsilon)>\sigma_e(\varepsilon)$.

Figure 9 shows the calculated C_2F_4 elastic and momentum transfer cross sections. The latter is expected to be somewhat inaccurate below about 10 eV.

The ionization rate coefficient is defined as

$$k_i=(2e/m)^{1/2}\int\sigma_i(\varepsilon)f_0(\varepsilon,E/N)\varepsilon\,d\varepsilon, \tag{6}$$

where σ_i is the ionization cross section. The ionization coefficient measured in a swarm experiment is

$$=k_iN/V_d, \tag{7}$$

which is the increase in electron density per centimeter due to ionization as a swarm of electron drifts against an electric field. This is usually displayed as $/N$ with units of cm^2.

The connection to microscopic electron collision physics is made explicitly through the momentum transfer cross section $\sigma_m(\varepsilon)$ and the electron energy distribution function $f_0(\varepsilon)$. The latter is the solution to Boltzmann's equation for electron transport in a plasma. All the microscopic physics implicit in the electron transport or swarm coefficients appears in Boltzmann's equation as dependencies on the electric field; gas, ion, and electron densities; and all elastic and inelastic collision cross sections (see the review by Morgan).[18] Boltzmann's equation can be solved numerically,[19] and the numerical solutions can be used in deducing electron collision cross sections from a set of measured electron transport coefficients. We use the two-term spherical harmonic approximation to the solution of Boltzmann's equation.[19] Further discussion of this approximation appears below. Because we solve for the steady-state electron energy distribution function $f_0(\varepsilon)$ by integrating an equation for $df_0(\varepsilon,t)/dt$ in time, we are able to include the effects of ionization and attachment on $f_0(\varepsilon)$. Attachment removes electrons preferentially from parts of $f_0(\varepsilon)$, and ionization produces low-energy secondary electrons that tend to increase $f_0(\varepsilon)$ at low energies. These processes, of course, can then affect the calculated transport coefficients. The smaller the value of E/N, the greater the effects of attachment and, conversely, the greater the value of E/N, the greater the effects of ionization and secondary-electron production on $f_0(\varepsilon)$ and the swarm coefficients. These effects have been pointed out by Tagashira[6,20] and have been addressed by him via a different mathematical and numerical technique from that used here.

In order to include secondary electron production in the solution of Boltzmann's equation, we use an ionization cross section $\sigma_i(\varepsilon_p,\varepsilon_s)$, which is the cross section for the production of a secondary electron in the energy range $0 \leqslant \varepsilon_s \leqslant (\varepsilon_p - I_p)/2$ for a primary electron having energy $\varepsilon_p \geqslant I_p$, where I_p is the ionization potential. $\sigma_i(\varepsilon_p,\varepsilon_s)$ has been measured for some gases[21] and analytic functional fits have been made for a number of gases.[22] In the absence of such a measured or calculated cross section, as is the present situation with C_2F_4, we choose $\sigma_i(\varepsilon_p,\varepsilon_s)$ to be a uniform function over the interval $0 \leqslant \varepsilon_s \leqslant (\varepsilon_p - I_p)/2$. This is an adequate approximation unless the value of E/N is so large that secondary electrons are added to $f_0(\varepsilon)$ at a rate faster than the energy exchange collision frequency for relaxing $f_0(\varepsilon)$.

Tagashira[6,20] has also written extensively on different definitions of drift velocity and how they yield different values depending upon the measurement or calculation being performed. He noted that drift velocities measured by mean-arrival-time, pulsed Townsend, and steady-state Townsend techniques can yield substantially different results at high values of E/N. We will elaborate further upon this below while discussing our measurements and calculations and other swarm measurements in C_2F_4.

Swarm analyses can be performed in a variety of ways. The most common method, historically, is to postulate a set of cross sections and manipulate their energy dependencies and magnitudes such that transport coefficients computed by solving Boltzmann's equation agree with measured values. Since we have available to us state-of-the-art *ab initio* calculations of the momentum transfer and electronic excitation cross sections and high-quality ionization cross section measurements, we have previously also used the approach of adding some model vibrational excitation cross sections to the set to take into account energy loss at low values of E/N and then adjusting the magnitudes of the cross sections to achieve consistency with measured swarm coefficients.

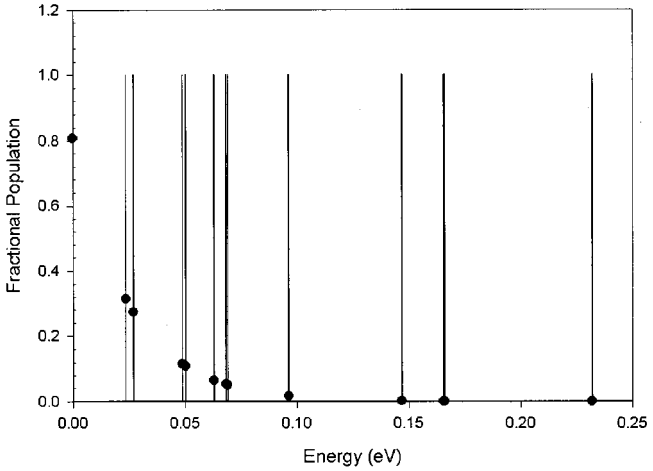

FIG. 10. C_2F_4 vibrational spectrum.

We have used the Born approximation forms for our model vibrational excitation cross sections. The Born expression[23] for vibrational excitation, which is commonly used, is

$$\sigma^B(v \rightarrow v') = (8\pi/3k_0^2)|\langle v'|d(R)|v\rangle|^2 \times \ln[(k+k')/|k-k'|], \tag{8}$$

where $d(R)$ is the dipole operator, v and v' are the initial and final vibrational quantum numbers, respectively, and k and k' are at the initial and final electron wave vectors. The wave vector and the kinetic energy are related by

$$k^2 = 8\pi^2 m/h^2 \varepsilon. \tag{9}$$

If $\Delta\varepsilon$ is the vibrational excitation energy in eV and ε is the electron impact energy, the Born approximation cross section for excitation is

$$\sigma_V^B = 3.7\times 10^{-15}/(\Delta\varepsilon x)\ln[(x^{1/2}+(x-1)^{1/2})/|x^{1/2}-(x-1)^{1/2}|], \tag{10}$$

where $x = \varepsilon/\Delta\varepsilon$ and the normalization is such that the peak value of σ_V^B is 1×10^{-16} cm^{-2}. Because we adjust the magnitudes of the vibrational excitation cross sections to give agreement with the measured swarm data, it is only the energy dependence of the Born cross section that is of interest to us.

The vibrational energy spectrum for C_2F_4 is shown in Fig. 10.[24] Also shown are the fractional populations of the vibrational levels at a temperature of 300 K. About 20% of the C_2F_4 molecules are vibrationally excited. Were we concerned with detailed low energy cross sections and transport coefficients at low values of E/N. We would need to account

in our solution of Boltzmann's equation for electron superelastic collisions, whereby the electrons gain energy in collisions with the vibrationally excited states.

We have used in our analysis two vibrational levels for C_2F_4 having energies of 0.16 and 0.23 eV. We use the downhill simplex and simulated annealing algorithms,[25,26] in our swarm analysis[27,28] in order to adjust the magnitudes and shapes of the cross sections to achieve a minimum in the rms difference between the sets of measured and computed transport coefficients.

B. Results of swarm analysis

1. Boltzmann's equation and the downhill simplex

We first tried using the measured ionization and the calculated momentum transfer and excitation cross sections in our swarm analysis, merely scaling the magnitudes of the cross sections in order to fit the measured swarm data as we did in our work on CHF_3.[29] This approach gave unrealistic results for the excitation cross sections, so we returned to the more sophisticated approach of adjusting both the energy dependencies and the magnitudes of the cross sections.

We began the analysis with the *ab initio* computed momentum transfer and total excitation cross sections, which were to be varied. The measured ionization cross sections were not varied but were included in the swarm calculations. The two model vibrational cross sections, each with a peak value of 10^{-16} cm^2, were included in the calculation as a check of their potential significance. For this analysis we used only the swarm data for $E/N \geqslant 300$ Td and did not expect low-energy vibrational excitation cross sections to contribute significant electron energy loss.[30]

The downhill or creeping simplex algorithm is a very versatile method for optimization problems of the kind where we desire to find the minimum of a function of n variables $y=f(x_1,x_2,\ldots,x_n)$. We can think of the function f as defining an n-dimensional surface in a space of $n+1$ dimensions. $n+1$ points on this surface then define what is called a *simplex*. The algorithm manipulates this simplex in order to contract it in all dimensions toward a minimum value. A simulated annealing algorithm is used concurrently as a means of avoiding minimizing into a local but not global minimum.

The function that we try to minimize is the mean square of the differences between the calculated and measured transport coefficients

$$\chi^2=\sum_i \{[(V_d^c-V_d^m)/V_d^m]^2+[(\alpha^c-\alpha^m)/\alpha^m]^2\}, \qquad (11)$$

where c and m denote calculated and measured drift velocities (V_d) and ionization coefficients α, which are functions of $(E/N)_i$. The sum is over all values of $(E/N)_i$. The momentum transfer and total excitation cross sections are given at a combined total of 54 energy points. The simplex then consists of the function χ^2 at $n+1=55$ independent points. We generated the initial set of 55 independent cross section vectors by a randomization process starting with the calculated cross sections. The calculation then proceeded with the manipulation of the 55 cross section vectors in order to shrink the 54-dimensional hyperplane defined by the values of χ^2 to a point at the minimum of the hypersurface.

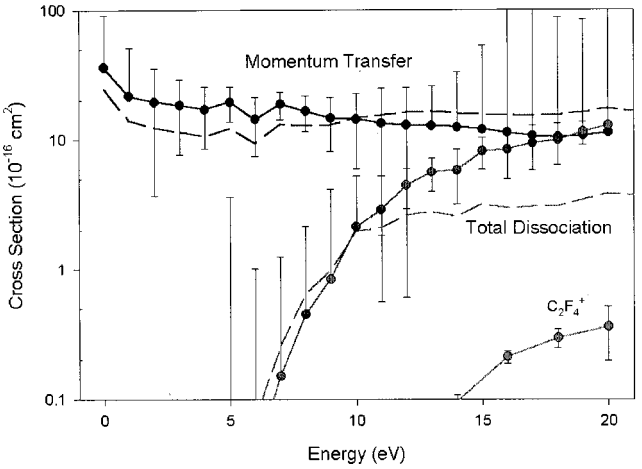

FIG. 11. Cross sections for momentum transfer and total dissociation and error bars derived from swarm analysis compared to *ab initio* calculations.

The momentum transfer and total excitation cross sections obtained for C_2F_4 from the simplex minimization algorithm are shown in Fig. 11. The calculated cross sections are also shown on the same graph. We find a momentum transfer cross section that is slightly larger than the calculated curve below 9 eV and somewhat smaller above 9 eV.

Because the total excitation cross section represents the sum of ten or more individual cross sections, we used a continuous energy loss rather than a fixed energy loss for inelastic collisions between electrons and C_2F_4. Our derived total inelastic cross section agrees well with the calculated values in the range from its 5 eV threshold to 11 or 12 eV and is then significantly larger. The fit to the measured swarm data is shown in Fig. 12.

2. Sensitivity analysis

It is rare in the field of swarm analysis to see an attempt to relate the uncertainty in measured transport coefficients to

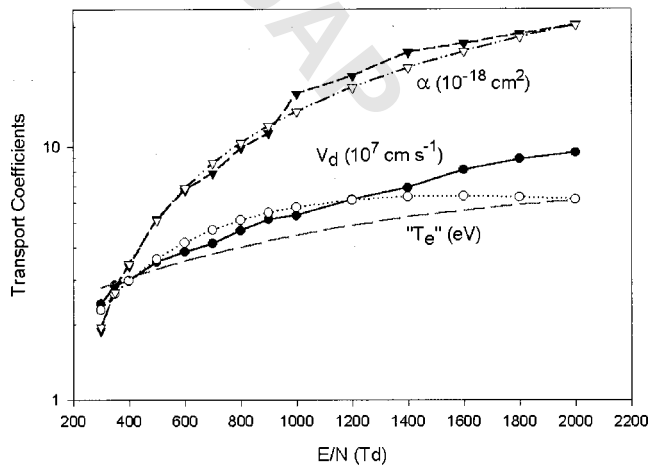

FIG. 12. Comparison of transport coefficients calculated using derived cross sections with measurements. The solid symbols are measurements and the open symbols are calculations. T_e is computed from $2\langle e\rangle/3$.

uncertainty in derived cross sections. Two elementary analytic examples can be used to explain the concept.

The first example is the limiting case of elastic scattering only with a constant collision frequency

$$\nu = v\,\sigma_m(v)N = \text{constant}, \tag{12}$$

which clearly occurs if $\sigma_m(v) \propto 1/v$. This gives rise to a Maxwellian electron speed distribution. The drift velocity in this example is

$$V_d = eE/m\,\nu \propto 1/\sigma_m\,. \tag{13}$$

So, in deriving σ_m from V_d, any uncertainty of ε in V_d implies an uncertainty of ε in σ_m.

The second example is the limiting case of elastic scattering only with a constant collision cross section σ_m. This gives rise to the Druyvesteyn electron speed distribution, where the drift velocity is given by

$$V_d \propto (eE/N\sigma_m)^{1/2}. \tag{14}$$

The uncertainty in a cross section derived from a measured drift velocity would hence be proportional to the square of the uncertainty in V_d. A 5% uncertainty in V_d, for example, becomes a 10% uncertainty in σ_m.

There is an additional lack of uniqueness, which was alluded to by Huxley and Crompton.[31] Our swarm data go to a maximum value of E/N of 2000 Td. Associated with this is some mean electron energy. Clearly transport coefficients will be insensitive to collisional processes in the tail of the distribution at energies several times the mean. Consequently, the derived cross sections at these energies will be very uncertain.

We have been able to put error bars on the derived cross sections based on estimated error bars for the swarm measurements. Clearly there must be uncertainty in the swarm derived cross sections because of uncertainty in the data and because swarm coefficients at any given value of E/N are themselves insensitive to cross section values outside of a somewhat narrow range of electron energy. We have obtained the error bars shown by varying each energy point of the cross sections and calculating the resulting change in the rms fit to the swarm data. In order to compute the error bars shown, we have assumed a $\pm 3\%$ uncertainty in the measured drift velocities and ionization coefficients. The error bars on the measured ionization cross section indicate how much variability would be allowed within the assumed $\pm 3\%$ uncertainty of the swarm data.

The derived total dissociation cross section rises to unrealistically large values above about 12 eV. We suspected that this was due to a loss of validity at high E/N of the two-term spherical harmonic solution to Boltzmann's equation.

3. Discussion of the two-term expansion

The two-term spherical harmonic expansion has been the approximation technique used for many decades for solving Boltzmann's equation for electrons in a gas. The velocity distribution function $f(\mathbf{v})$ is expanded into a spherically symmetric component $f_0(v)$ and a vector component $\mathbf{f}_1(v)$ in the $\mathbf{E}$ field direction such that

$$f(v) \cong f_0(v) + (\mathbf{v}/v)\cdot\mathbf{f}_1(\mathbf{v}) \cong f_0(v) + |\mathbf{f}_1(v)|\cos\theta. \tag{15}$$

This approximation works extremely well for small to moderate fields where

$$|\mathbf{f}_1| \ll f_0\,. \tag{16}$$

Reducing Boltzmann's transport equation using this approximation and assuming steady state and spatial homogeneity,

$$e\mathbf{E}/m\cdot\boldsymbol{\nabla}_v f(v) = (\partial f/\partial t)_{\text{coll}},$$

yields a scalar equation for f_0 and the following vector equation relating f_0 and $\mathbf{f}_1$:

$$e/m\mathbf{E}/N\,df_0(v)/dv = 2\pi v\,\mathbf{f}_1(v)\int \sigma_e(v,\theta) \times(1-\cos\theta)\sin\theta\,d\theta \tag{17a}$$

$$= v\,\sigma_m(v)\mathbf{f}_1(v), \tag{17b}$$

where σ_m is the momentum transfer cross section defined as a weighted integral of the differential elastic scattering cross section. Clearly, the integral of $\mathbf{f}_1$ over all speeds is the electron drift velocity in the direction of the electric field.

The requirement that $|\mathbf{f}_1| \ll f_0$ then amounts to stating that the electron drift velocity must be much smaller than the random thermal speed of the electrons for the two-term approximation to be valid. Looking at Fig. 12, we see that $V_d \cong 10^8$ cm/s at $E/N = 2000$ Td. If the reduced mean energy $2\langle e\rangle/3$ is about 10 eV, as shown in Fig. 12, the thermal speed is then only twice the drift velocity. We can expect the two-term approximation to be inaccurate under such conditions.

Baraff and Buchsbaum[32] explored the breakdown of the two-term approximation, finding that, at high values of E/N, "the distribution function is sufficiently anisotropic that it cannot be represented by a two-term expansion in spherical harmonics." What constitutes high E/N depends, of course, on the gas in question. This was further elaborated upon by Phelps and Pitchford,[33] who showed that the breakdown of the two-term approximation, where the angular dependence of elastic scattering is entirely contained within the definition of the momentum transfer cross section [as shown in Eqs. (5) and (14a) and 14(b)] leads to a more explicit dependence of the distribution function on the degree of anisotropy of the differential scattering cross sections. We can see in Fig. 13 that for even relatively low collision energies the differential elastic cross sections are very anisotropic.

Although the two-term approximation worked well in CHF_3 swarm analysis,[29] here we are working with values of E/N approximately ten times the values used in that work. A similar situation can be found in swarm analyses of electrons in SF_6. Itoh *et al.*[34] have found, using two-term and three-term expansions of Boltzmann's equation, that the two-term approximation, as we have seen here, becomes increasingly inaccurate with E/N for values about 1000 Td. Because of this we resort to Monte Carlo simulations in our C_2F_4 swarm analyses.

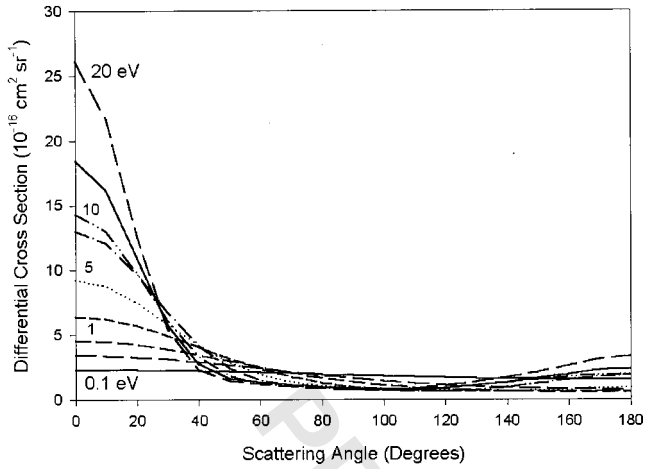

FIG. 13. Differential elastic scattering cross sections for electrons in C_2F_4. Cross sections are shown for collision energies of 0.1, 0.5, 1.0, 2.0, 5.0, 7.5, 10.0, 15.0, and 20.0 eV.

4. Monte Carlo simulations

We have repeated the swarm calculations using a Monte Carlo simulation of the electron transport process. Now, instead of the momentum transfer cross section, we use the differential elastic cross section $\sigma_e(\varepsilon,\theta)$ and the total elastic cross section in the simulation

$$\sigma_e(\varepsilon)=2\pi\int \sigma_e(\varepsilon,\theta)\sin\theta\, d\theta. \tag{18}$$

Selected results for $\sigma_e(\varepsilon,\theta)$ are plotted in Fig. 13. Forward scattering dominates for energies greater than several eV. This is consistent with the relative values of $\sigma_e(\varepsilon)$ and $\sigma_m(\varepsilon)$ shown in Fig. 9.

We perform a direct simulation of the swarm experiment using a three-dimensional Monte Carlo program. The transport coefficients are obtained by sampling the trajectories of the electrons in space and time. The drift velocity is obtained by sampling the electron arrival times, and the ionization coefficient is obtained by counting the number of ionizations over a distance in the direction of drift.

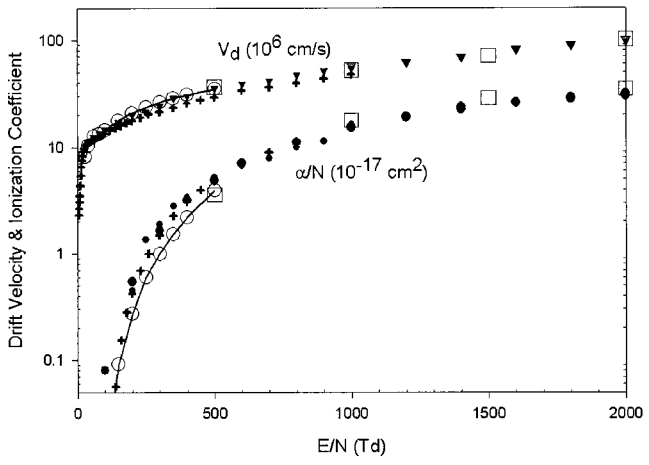

FIG. 14. Measured and calculated electron swarm data: (filled symbols) measured values of V_d and α/N, (+) measurements of Goyette *et al.* (Ref. 1), (open circles) calculated using the two-term approximation to Boltzmann's equation, and (open squares) results of Monte Carlo simulations.

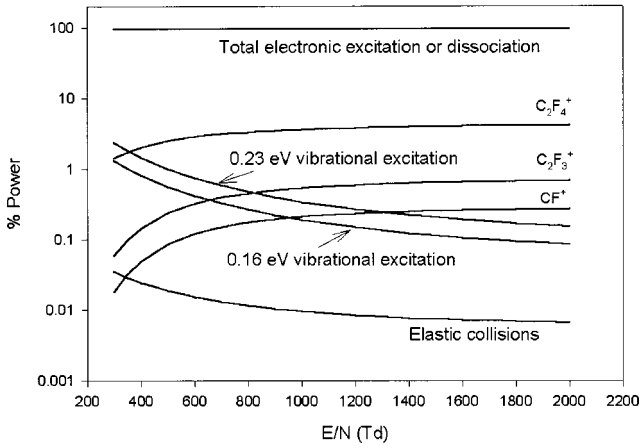

FIG. 15. Electron power flow in collisions with C_2F_4.

The Monte Carlo simulation results are shown in Fig. 14 at 500, 1000, 1500, and 2000 Td. They can be seen to be in excellent agreement with the measured drift velocities and ionization coefficients. The quality of this agreement demonstrates the accuracy of the combination of *ab initio* elastic and excitation cross sections plus measured ionization cross sections for average electron energies above about 5 eV.

5. Estimate of vibrational excitation cross sections

We have successfully employed the combination of two term spherical harmonic approximation to the solution of Boltzmann's equation and the downhill simplex optimization algorithm to extract estimates for C_2F_4 vibrational excitation cross sections using swarm data for $30\,\text{Td}\leqslant E/N\leqslant 500\,\text{Td}$. The energy dependence of each cross section is described by Eq. (11). They have energy losses of 0.16 and 0.23 and peak values of 11.7×10^{-16} and 5.2×10^{-16} cm^2, respectively. The calculated swarm coefficients are shown in Fig. 14. They agree very well with the Monte Carlo results at $E/N=500\,\text{Td}$.

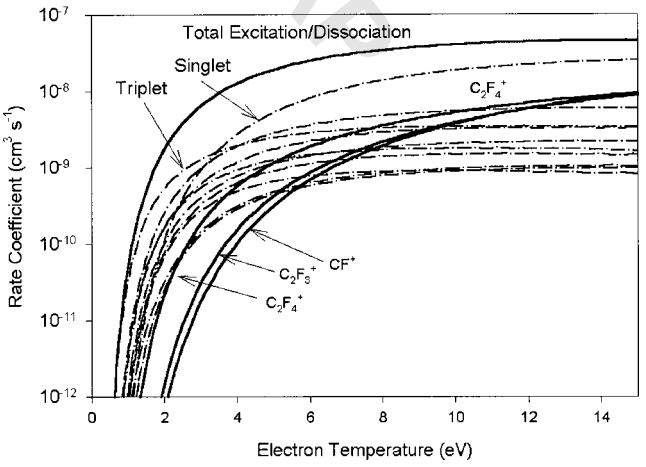

FIG. 16. Rate coefficients for excitation and ionization of C_2F_4.

As can be seen from Fig. 15, which shows where electron energy is lost in collisions with C_2F_4, more than 90% of the energy loss for electrons in the temperature range of 2–5 eV is to electronic excitation and dissociation. Only a few percent, even at 200 Td, goes into vibrational excitation.

6. Summary of cross section set

The close agreement between the results of the Monte Carlo simulation and the measured swarm parameters justifies employing the measured ionization cross sections[17] and the calculated neutral excitation cross sections without further adjustment in the final cross section set. Above 5 eV, elastic scattering likewise is represented via the calculated differential elastic cross section without adjustment. Below 5 eV, the Born approximation vibrational excitation cross sections described in Sec. III B 5 are significant, while elastic scattering should be accounted for via the adjusted momentum transfer cross section shown in Fig. 11.

7. Remarks on other swarm measurements

Goyette *et al.*[1] very recently published measurements of electron drift velocity, ionization coefficient, and attachment rate coefficient in C_2F_4 over an E/N range of 7 Td to 1000 Td. In the 200–1000 Td overlap region between their measurements and ours, their pulsed Townsend results and our arrival time results are in very good agreement. This comparison, along with the excellent agreement between our calculated results at 500 Td using two different techniques, gives us confidence in the accuracy of our analysis.

Goyette *et al.* observed in their measurements of $(\alpha\text{-}\eta)/N$ (the difference between the ionization and attachment coefficients) as a function of E/N that there is a transition from net attachment to net ionization at a value of $E/N \cong 130$ Td. As our ionization coefficient measurements were performed for values of $E/N \geqslant 200$ Td, this observation is consistent with ours, stated in Sec. II A 1, that electron attachment is negligibly small in C_2F_4. The authors deduce a rate coefficient for attachment that is about $8\times10^{-11}\,\mathrm{cm}^3/\mathrm{s}$ at $E/N=4.5$ Td and falls to a value of $4\times10^{-12}\,\mathrm{cm}^3/\mathrm{s}$ at $E/N=100$ Td. Goyette *et al.*[1] present an extensive discussion of issues surrounding the conflicting measurements and calculations pertinent to electron attachment processes in C_2F_4.

C. Rate coefficients and fits

Figure 16 shows the rate coefficients for excitation and ionization of C_2F_4. The ten individual excitation cross sections are shown without labels. The curves labeled "Triplet" and "Singlet" refer, respectively, to the $1\,^3B_{1u}$ and $1\,^1B_{1u}$ excitations, the latter having a large oscillator strength. The rate coefficient computed using the sum of all ten cross sections is also shown.

The rate coefficients for electron collisions with C_2F_4 have been fitted to the Arrhenius form

$$k(T_e)=\alpha T_e^{\beta}\exp[-\gamma/T_e]\ \ \mathrm{cm}^3/\mathrm{s}, \tag{19}$$

where T_e is the electron temperature in eV. Table II lists the parametrized rate coefficients.

TABLE II. Parametrized rate coefficients for electron collisions in C_2F_4.[a]

Product	α	β	γ
Total excitation:	3.297 (−08)	4.118 (−01)	6.329 (+00)
Ten individual excitations:			
$1\,^3B_{1u}$ (T)	1.315 (−08)	−3.107 (−01)	5.994 (+00)
$1\,^1B_{1u}$ (V)	4.668 (−08)	1.467 (−01)	1.225 (+01)
$1\,^3B_{1g}$	9.046 (−09)	−8.641 (−02)	7.773 (+00)
$1\,^1B_{1g}$	2.567 (−09)	−1.643 (−02)	8.590 (+00)
$1\,^3B_{3u}$	2.267 (−08)	−7.106 (−01)	8.909 (+00)
$1\,^1B_{3u}$	1.984 (−08)	−1.785 (−01)	8.458 (+00)
$1\,^3A_g$	2.924 (−08)	−1.043 (+00)	1.068 (+01)
$1\,^1A_g$	1.724 (−08)	−5.071 (−01)	9.592 (+00)
$1\,^3B_{2g}$	1.743 (−08)	−6.257 (−01)	9.905 (+00)
$1\,^1B_{2g}$	8.130 (−09)	−4.784 (−01)	1.084 (+01)
Ionization:			
CF^+	5.874 (−09)	6.188 (−01)	1.929 (+01)
$C_2F_3^+$	3.025 (−09)	8.240 (−01)	1.641 (+01)
$C_2F_4^+$	3.583 (−09)	6.613 (−01)	1.106 (+01)

[a]The notation $(\pm xx)$ indicates $\times10^{\pm xx}$.

V. SUMMARY AND CONCLUSIONS

We have presented results of swarm measurements, first-principles cross section calculations, and swarm analyses for electrons in C_2F_4. Using the data presented herein and measured ionization cross sections, the swarm analysis has allowed us to assemble a self-consistent, validated set of cross sections for electron impact on C_2F_4. We expect this cross section set to be useful to those simulating the plasma chemistry of C_2F_4 discharges. The process of validation of a cross section set using the swarm analysis procedure presented above ensures the self-consistency needed to yield correct predictions of plasma electrical conductivity, ionization state, and rate of radical production due to dissociation of the parent gas, C_2F_4 in this case.

ACKNOWLEDGMENTS

The authors would like to thank Dr. Peter Ventzek of Motorola, Inc., for his interest in and encouragement of this work. Work at Caltech was supported by the Office of Basic Energy Sciences of the U.S. Department of Energy, by Sematech, Inc., and an equipment grant from Intel Corp.

[1] A. N. Goyette, J. de Urquijo, Y. Wang, L. G. Christophorou, and J. K. Olthoff, J. Chem. Phys. **114**, 8932 (2001).
[2] S. Samukawa and T. Mukai, J. Vac. Sci. Technol. A **17**, 2551 (1999).
[3] K. Yoshida, N. Sasaki, H. Ohuchi, H. Hasegawa, M. Shimozuma, and H. Tagashira, J. Phys. D **32**, 862 (1999).
[4] H. Tagashira, Technical Papers of Electrical Discharge Committee IEE Japan, 1985, ED-85-115.
[5] K. Kondo and H. Tagashira, J. Phys. D **23**, 1175 (1990).
[6] H. Tagashira, Y. Sakai, and Sakamoto, J. Phys. D **10**, 1051 (1977).
[7] K. Yoshida, T. Ohshima, Y. Ohmori, H. Ohuchi, and H. Tagashira, J. Phys. D **29**, 1209 (1996).
[8] Swarm data for CF_4 and C_2F_6: http://www.eeel.nist.gov/811/refdata/
[9] Swarm data for C_2H_4: W. L. Morgan (private communication).
[10] K. Takatsuka and V. McKoy, Phys. Rev. A **24**, 2473 (1981).
[11] K. Takatsuka and V. McKoy, Phys. Rev. A **30**, 1734 (1984).
[12] C. Winstead and V. McKoy, Adv. At., Mol., Opt. Phys. **36**, 183 (1996).
[13] C. Winstead, C.-H. Lee, and V. McKoy, in *Industrial Strength Parallel Computing: Programming Massively Parallel Processing Systems*, edited by A. Koniges (Morgan-Kaufmann, 2000), p. 247.

[14] C. Winstead and V. McKoy, J. Chem. Phys. (in press).
[15] M. J. Coggiola, W. M. Flicker, O. A. Mosher, and A. Kuppermann, J. Chem. Phys. **65**, 2655 (1976).
[16] G. Bélanger and C. Sandorfy, J. Chem. Phys. **55**, 2055 (1971).
[17] P. D. Haaland and C. Jiao (private communication).
[18] W. L. Morgan, Adv. At., Mol., Opt. Phys. **43**, 155 (2000).
[19] W. L. Morgan and B. M. Penetrante, Comput. Phys. Commun. **58**, 127 (1990).
[20] H. Tagashira, in *Swarm Studies and Inelastic Electron-Molecule Collisions*, edited by L. C. Pitchford, B. V. McKoy, A. Chutjian, and S. Trajmar (Springer, New York, 1987).
[21] C. B. Opal E. C. Beaty and W. K. Peterson Joint Institute for Laboratory Astrophysics Report No. 108, University of Colorado, May 26, 1971; At. Data **4**, 204 (1972).
[22] A. E. S. Green and T. Sawada, J. Atmos. Terr. Phys. **34**, 1719 (1972).
[23] N. F. Lane, Rev. Mod. Phys. **52**, 29 (1980).
[24] M. W. Chase, Jr., 4th J. Phys. Chem. Ref. Data Monogr. **9**, ■■■ (1998).
[25] W. H. Press, S. A. Teukolsky, W. T. Vetterling, and B. P. Flannery, *Numerical Recipes in Fortran 77*, 2nd ed. (Cambridge University Press, New York, 1992).
[26] N. Gershenfeld, *The Nature of Mathematical Modeling* (Cambridge University Press, New York, 1999).
[27] W. L. Morgan, Phys. Rev. A **44**, 1677 (1991).
[28] W. L. Morgan, J. Phys. D **26**, 209 (1993).
[29] W. L. Morgan, C. Winstead, and V. McKoy, J. Appl. Phys. **90**, 2009 (2001).
[30] We employed Gaussian model cross sections to investigate the possible effects of vibrational resonances at 3, 7, and 10eV, but the results were inconclusive.
[31] L. G. H. Huxley and R. W. Crompton, *The Diffusion and Drift of Electrons in Gases* (Wiley, New York, 1974).
[32] G. A. Baraff and S. J. Buchsbaum, Phys. Rev. **130**, 1007 (1963).
[33] A. V. Phelps and L. C. Pitchford, Phys. Rev. A **31**, 2932 (1985), and references therein.
[34] H. Itoh, M. Kawaguchi, K. Satoh, Y. Miura, Y. Nakao, and H. Tagashira, J. Phys. D **23**, 299 (1990).